Anisotropies in the electrical properties of rod-like aggregates of liquid crystalline phthalocyanines: Direct current conductivities and field-effect mobilities

Carrie L. Donley,[a] R.A.P. Zangmeister,[b] Wei Xia, Britt Minch, and Anthony Drager
Department of Chemistry, University of Arizona, Tucson, Arizona 85721

Samir K. Cherian, Lynn LaRussa, Bernard Kippelen,[c] Benoit Domercq,[c] and David L. Mathine[d]
Department of Optical Sciences and Department of Electrical and Computer Engineering, University of Arizona, Tucson, Arizona 85721

David F. O'Brien and Neal R. Armstrong[d]
Department of Chemistry, University of Arizona, Tucson, Arizona 85721

(Received 4 November 2003; accepted 12 April 2004)

The direct current (dc) conductivities and organic field-effect transistor (OFET) characteristics of a class of octa-substituted liquid crystalline (discotic mesophase) phthalocyanines (Pcs) are discussed. These molecules self-organize into columnar aggregates with large coherence lengths (up to approximately 300 nm). Langmuir–Blodgett films of these molecules were horizontally transferred to either interdigitated microelectrodes (IME) or OFET substrates, so that current flow could be measured either parallel or perpendicular to the column axis. Twenty-eight bilayer films of these Pcs on the IME substrates showed anisotropies in dc conductivity up to 50:1, whereas similar Pc films showed anisotropies in field effect mobilities of approximately 10:1, for a variety of W/L ratios (source/drain dimensions and spacing). Field-effect mobilities of 1 to 5×10^{-6} $cm^2 \cdot V^{-1} \cdot s^{-1}$ were determined from OFET measurements, along the Pc column axis, whereas charge mobilities measured from the space charge limited current regime on the IME substrates were in the range of 10^{-4} $cm^2 \cdot V^{-1} \cdot s^{-1}$. Conductive tip atomic force microscopy measurements on the apprximately 500-nm length scale showed that the conductivity anisotropy can be as high as 1000:1 when the Pc columns are intimately contacted to an adjacent Au bond pad.

I. INTRODUCTION

Many liquid crystalline discotic mesophase materials self-organize from common solvents into coherent columnar, rod-like aggregates, and have become of interest as potential solution-processed molecular electronic materials.[1–20] Side-chain modified phthalocyanines, porphyrins, hexabenzocoronenes, and triphenylenes have been created that show reasonable liquid crystalline (LC) transition temperatures ($K \rightarrow D_h$) and can be readily processed into thin films. The side chains surrounding the discotic molecular core help control self-organization into these rod-like columns, and because of their close-packing and electrically insulating nature, their presence may eventually provide for dense lateral integration of organic field-effect transistor (OFET) devices, preventing significant electrical cross-talk between adjacent columns. These side chains, however, may also create an additional energy barrier to charge injection into the rod-like aggregate, if charge injection is not directly into the macrocycle core, and may complicate the formation of ohmic contacts to these materials.

For many of these materials, thin films are formed with the column axis of the rod-like aggregate parallel to the substrate plane, the preferred orientation for optimized charge transport in an OFET.[10,17–35] The electrical properties of some of these materials have been characterized using time-of-flight, direct current (dc) conductivity, or time resolved-pulsed radiolysis microwave conductivity methods, and charge mobilities arising from these measurements appear to be larger along the rod axis

[a]Current address: Cavendish Laboratory, University of Cambridge, Cambridge CB3 0HE, England.
[b]Current address: National Institute for Standards and Technology, Gaithersburg, MD.
[c]Current address: Electrical Engineering, Georgia Tech University, Atlanta, GA 30332.
[d]Address all correspondence to these authors.
e-mail: nrau.arizona.edu
DOI: 10.1557/JMR.2004.0278

versus perpendicular to that axis. These mobilities are also critically dependent on the coherence of the aggregate, and the length scale over which the electrical properties are measured.[1–5,12–14,17–20]

As will be discussed in this report, there are significant challenges yet to be overcome in optimizing the electrical properties of discotic mesophase materials for OFET applications. First, the charge mobilities in these discotic materials are strongly affected by misalignments, bifurcations, and breaks in the columnar aggregates (reminiscent of grain boundaries in crystalline materials),[25–29] which constitute a high-resistance pathway for charge migration. The coherence and electrical properties of these assemblies are strongly influenced by the chemical and physical nature of their interface with the substrate, as the region of the organic semiconductor closest to the gate oxide is where most of the charge will flow in an OFET.[21] Last, making ohmic, conformal contacts between the source and drain electrode, and the ends of these columnar aggregates is not straightforward, and as will be shown, significant gains are required in the optimization of these contact regions.

The specific molecules discussed here (2,3,9,10,16,17,23,24-octakis(2-benzyloxyethoxy) phthalocyaninato-copper ($CuPc(OCH_2CH_2OBz)_8$—Pc **1**), 2,3,9,10,16,17,23,24-octakis(2-benzyloxyethoxy) phthalocyaninato-cobalt ($CoPc(OCH_2CH_2OBz)_8$—Pc **1'**), and 2,3,9,10,16,17,23,24-octakis((2-cinnamyl)ethoxy)phthalocyaninato copper (II) (abbreviated $CuPcOCH_2CH_2OCH_2CH=CHPh)_8$, Pc **2**) are members of a series of octa-substituted phthalocyanines we have recently developed (Fig. 1).[17–20,36] Their benzyl-oxy-ethoxy side chains have been seen to impart unusual coherence to the columnar aggregates that form spontaneously in condensed phases. These phthalocyanines (Pcs) form well-ordered Langmuir–Blodgett (LB) thin films containing parallel columnar aggregates with a center-to-center spacing of these rod-like aggregates of 2.7–3.1 nm, which can be horizontally transferred to hydrophobized substrates as intact films. The coherence of these rod-like aggregates often exceeds 150 nm [e.g., region (a) in AFM image of Fig. 1], which appears to arise because of the summation of the Pc ring–ring interactions and the interaction of the eight benzyl-terminated ethylene oxide side chains. Modification of the terminal benzyl groups for Pc **1** to include a styryl group at the termination of the side chain leads to Pc **2**.[17] Irradiation of the multilayer films of Pc **2** at 254 nm creates cylcobutane links between adjacent Pcs and provides for stabilization and lithographic patterning of the Pc film. Polymerization of films of **2** may lead to increased coherence lengths of the Pc column, fewer defects, and increased mobility. In both the parent Pc and in the polymerizable versions there are, however, significant populations of disordered material [region (b) in atomic force microscopy (AFM) image of Fig. 1] where discontinuities, bifurcations, and so forth, occur over several sets of columns, which are important to the discussion of the electrical properties of these materials (see below).

In this paper, we summarize the microcircuit-based electrical characterization (dc conductivities) and recently obtained OFET characterization of these Pc molecules. For thin films of all of these Pcs, it is shown that the dc conductivity parallel to the column axis ($\sigma_{\|}$) versus the conductivity perpendicular to the column axis ($\sigma_{\perp}$) shows ratios ($\sigma_{\|}/\sigma_{\perp}$) of 2–50 for conductivities measured on the 10-μm distance scale, with $\sigma_{\|}/\sigma_{\perp}$ increasing to 100–1000 when conductivities are measured on the submicrometer length scale using conductive-tip AFM. The mobilities obtained from space-charge limited current regime in the dc conductivity measurements are larger than those obtained for first-generation OFET devices. The OFET i/V curves are strongly sensitive to the chemical composition of the surfaces of the source and drain electrodes. The combination of these experiments confirm the critical role played by the coherence of the rod-like aggregates, and the formation of ohmic contacts to the ends of each Pc rod, in the further optimization of OFET circuits based on these materials.

II. EXPERIMENTAL

2,3,9,10,16,17,23,24-Octakis(2-benzyloxyethoxy)phthalocyaninato copper (II) (abbreviated $CuPc(OCH_2CH_2OBz)_8$, **1**), 2,3,9,10,16,17,23,24-Octakis(2-benzyloxyethoxy)phthalocyaninato cobalt (II) (abbreviated $CoPc(OCH_2CH_2OBz)_8$, **1'**), and 2,3,9,10,16,17,23,24-octakis(2-cinnamylethoxy)phthalocyaninato copper (II) (abbreviated $CuPcOCH_2CH_2OCH_2CH=CHPh)_8$, **2**) were synthesized as previously reported.[35] Solutions of these molecules were prepared in HPLC grade $CHCl_3$ stabilized with ethanol (Aldrich). Substrates were modified by exposing the clean surface to a 5% 1,1,1,3,3,3-hexamethyldisilazane, 5% 1,3-diphenyl-1,1,3,3-tetramethyldisilazane solution in $CHCl_3$, in an ultrasonic bath, for 30 min, with heating.

A Riegler & Kerstein RK3 Langmuir–Blodgett trough was used to form LB films with the Pc columns parallel to the compression barriers. This orientation of the Pc columns was maintained by using a horizontal (Schaefer) transfer of the segmented films to appropriately modified substrates.[37,38] Multilayer films were deposited to either interdigitated array microelectrodes (IMEs; 25 finger-pair Au microelectrodes 3 mm in length, with 10-μm spacing on silica substrates (Abtech)) or OFET substrates, one monolayer at a time (the most stable transfer conditions for films of **2**) or one bilayer at a time (the most stable transfer conditions for films of **1** and **1'**). A

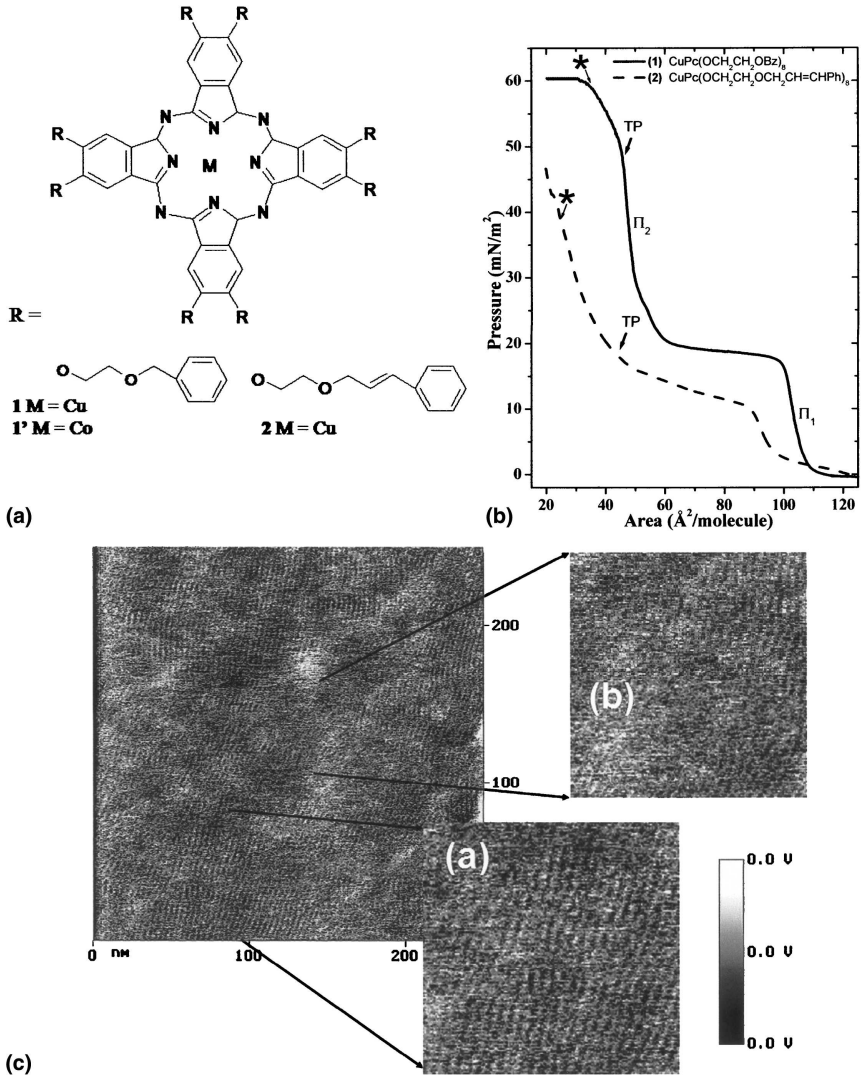

FIG. 1. (a) Structures of the octa-substituted phthalocyanine molecules examined in this study: **1** is the parent compound in a series of benzyl-oxy-ethoxy side chain modified Pcs (Refs. 18–20), and **2** is a recently introduced polymerizable version of this Pc, with stryl termination of the side chains (Ref. 17). (b) Pressure-area isotherms of **1** and **2** showing the phase transitions during film compression: **1** undergoes clear transitions from monolayer to compact bilayer, and films were transferred horizontally at that transition pressure. These transitions were less clear in **2**, but transfer of reasonably coherent rod-like aggregates of both molecules could still be achieved, at the points marked TP, as seen in the AFM image in (c). Two regions are shown in the AFM (friction, aqueous solution) images (Ref. 38). (a) in the AFM image corresponds to a region where Pc column coherence is approximately 100 nm or more and (b) in the AFM image corresponds to a region where column bifurcation and breaks in these columns are observed.

total of 28 bilayers of **1**, or **1'** or 28 monolayers of **2** were transferred to the IME substrates, and 7 bilayers of **1** or 7 monolayers of **2** were transferred to the OFET substrates. Residual water was removed from these samples with a stream of N_2 between each transfer step. Films were annealed in vacuum at 120 °C for at least 4 h to remove any trapped water and to induce further ordering within the film by annealing at a temperature above the liquid crystalline transition temperature for the material.[17–20] Following film transfer, the polymerization of films of **2** was carried out in an argon-purged environment with Hg-vapor pen lamps filtered to provide only 254-nm radiation.[17]

The dc conductivity experiments were conducted with a Keithley source meter (controlled by LabView software), in a N_2-gas purged environment, to minimize interference from adsorbed gases. The Pc-coated IME was held in this environment for several hours prior to measurement to provide for complete purging of adsorbed oxygen from the film surface. Conductivity values were

calculated from the current response of linear bias potential scans from 0 to 5 V at a 0.1 volt per second scan rate. Photoconductivities were determined from current/voltage scans in the ohmic potential region with irradiation from a HeNe laser (15 mW, 633 nm) or a Xe arc lamp (430 mW, 400–700 nm, IR filtered). Current-voltage responses at higher fields were recorded by cycling the potential from 0 to 50 V at a 1 volt per second scan rate. Temperatures were monitored in the photoconductivity experiments with a thermocouple mounted behind the samples to insure that increases in current were not simply the result of local heating of the microcircuit.

Dark conductivity measurements on the submicrometer distance scale were made using a Veeco-Digital Instruments Dimension 3100 SPM system, using a Pt/Ir tip on a cantilever with a force constant of 0.2 N/m. Four bilayer films of **1** were deposited on 100 nm SiO_2 on Si(100) substrates with 100 nm height Au pads (ca. 2 mm × 2 mm) spaced over the surface, providing flat oxide surfaces between the bond pads up to 2 mm × 2 mm in area. These oxide surfaces were chemically modified as described above, to optimize their hydrophobic character and the coherence of the Pc films. The Pt/Ir tip was positioned near the gold bond pad, at positions which would allow measurement of dark conductivities either parallel to the Pc column axis or perpendicular to that axis, in a region of the Pc film not more than approximately 5 μm away from the Au bond pad (see below). Current–voltage curves were obtained at several positions on the Pc film, as the tip was brought either successively closer or further away from the bond pad. In subsequent studies, we obtained images of current versus position on these thin films, with the current preamplifier set to record differences in current over the range from 0.2 to 2.0 pA.

All OFETs were fabricated on ⟨100⟩ *n*-type silicon substrates with a resistivity between 0.008 and 0.02 Ω·cm.[37] This highly doped silicon substrate was used as the gate electrode while a thermally grown 100-nm oxide layer over this substrate was used as the gate insulator. Electrodes were defined on the surface of the thermal oxide using standard photolithographic lift-off techniques to define Ti/Au (10 nm/100 nm) source and drain contacts. The surface was cleaned with an oxygen plasma at 100 W for 2 min to remove any residual photoresist. The source-drain widths available on each OFET chip were 10, 20, 50, 100, 200, 500, and 1000 μm, with the 200–1000-μm devices being the most commonly used for these studies. These devices had source-drain lengths of 1, 2, 3, 4, 5, 10, 20, and 50 μm. These width and length combinations result in a wide variety of width-to-length ratios (from 0.2 to 1000).

To avoid placing organic material on the upper surface of the gold source and drain contacts, the upper surfaces of the contacts were masked off with a black strippable paint. After the paint had dried (approximately 30 min), the samples were placed into a custom-made sample holder that allowed for two OFET chips to be mounted at the same time, either with the same orientation, or with orthogonal orientations (for anisotropy studies), whereupon horizontal transfer of the Pc LB films was conducted. Control experiments have shown that negligible contamination or damage to the Au contacts was created by the use of the black strippable paint.[38]

Following Pc film deposition on OFET substrates, the black strippable paint was peeled off, and the films were annealed in vacuum at 120 ° for 4 h and left in vacuum (usually overnight) until immediately before transport to the testing environment. Samples were placed in separate Nalgene jars in an argon purged and vacuum sealed (approximately 100 mTorr) dessicator for sample transport. The dessicator remained sealed until immediately before testing was to begin. These steps were taken to try to avoid excess doping of the films with oxygen, which was evident in the testing process over time.

For studies involving chemically modified source and drain electrodes, the entire OFET chip was first immersed in a 1 mM solution of 4-mercaptopyridine (Aldrich) in ethanol for at least 24 h. The chip was thin rinsed in ethanol, dried in a stream of nitrogen, and masked with the black strippable paint, as for the unmodified OFET circuits.

The OFET chips were tested with a custom probe station. Signatone micromanipulators were used to position tungsten probes onto the surface electrodes. An Agilent 4142B modular dc source/monitor was used to acquire the electrical data from the organic transistors. The ground channel was connected to a common source, and two separate channels were contacted to two separate transistor drains, which allowed the simultaneous testing of two transistors. Contact was made to the gate through a back-side gold contact in contact with a base plate that was under potential control. The source-drain voltage was then swept with a reduced sweep rate so that the low mobility transistors could respond. The source current monitor was interfaced with LabView software to control the scan voltages on both the drain and the gate.

III. RESULTS AND DISCUSSION

A. dc conductivities for Pcs 1 and 1'

Dark and photoconductivities of thin films of Pc **1**, **1'**, and **2** were first investigated using interdigitated array microelectrode circuits (IMEs; 10-μm spacing between electrodes) on silica substrates, which were surface-modified using a mixture of methyl- and phenyl-terminated silanes.[19] The results of these measurements are summarized in Table I. Similar studies of dc conductivity on IMEs have been reported by Neher and coworkers for rod-like silicon phthalocyanine polymers,[12–14]

TABLE I. Dark and photoconductivities (shown as ranges for all microcircuits studied) calculated for Pc **1** ($CuPc(OCH_2CH_2OBz)_8$) and Pc **1′** ($CoPc(OCH_2CH_2OBz)_8$) based on j-V response curves.[a]

	Pc **1** ($CuPc(OCH_2CH_2OBz)_8$)			Pc **1′** ($CoPc(OCH_2CH_2OBz)$		
	$\sigma_\perp$ (Scm^{-1})	$\sigma_\parallel$ (Scm^{-1})	$\sigma_\parallel/\sigma_\perp$	$\sigma_\perp$ (Scm^{-1})	$\sigma_\parallel$ (Scm^{-1})	$\sigma_\parallel/\sigma_\perp$
Dark	1×10^{-10}	2×10^{-10} to 5×10^{-9}	2 to 50	1×10^{-10} to 7×10^{-9}	2×10^{-9} to 8×10^{-8}	10 to 20
HeNe laser (15 mW)	6×10^{-10} to 2×10^{-9}	1×10^{-8} to 4×10^{-8}	17 to 23	2×10^{-10} to 5×10^{-9}	1×10^{-8} to 5×10^{-8}	10 to 70
Xe arc lamp (filterd, 430 mW)	5×10^{-9} to 8×10^{-9}	5×10^{-8} to 9×10^{-8}	6 to 17	2×10^{-10} to 7×10^{-9}	2×10^{-8} to 6×10^{-8}	8 to 98

[a]1×10^{-10} Scm^{-1} is the lowest conductivity that could be accurately measured using this approach. dc conductivities for thin films of **2** are detailed in Ref. 17.

and in our own preliminary work for Pc **1**.[20] Relatively thick (28 bilayers) multilayer thin films of Pcs **1** and **1'** and 28 monolayer films of Pc **2** were deposited onto two IMEs oriented orthogonal to each other during the horizontal deposition process, producing comparable Pc thin films from the same Langmuir layer with parallel and perpendicular orientations of the Pc column rod axes with respect to the legs of the microcircuit (inset of Fig. 2). AFM images of the transferred Pc films on these microcircuits reveal that each bilayer film is cut by the square profile Au microelectrode fingers (approximately 100-nm height) during the horizontal deposition so that the Pc film makes contact primarily to the sides of these microcircuit legs.[20] This may be significant both for these measurements, and for the OFET measurements below, as these Au fingers are deposited on the silica substrate using first an approximately 5-nm adhesion layer of Ti, which is likely oxidized prior to film deposition, so that the bottom Pc layers likely do not contact Au, and the upper Pc layers may make only intermittent contact with the Au pads.

Linear current–voltage plots were observed for all Pc films examined in the applied voltage range from 0 to approximately 10 volts [Figs. 2(a) and 2(b)], corresponding to applied fields of up to 10^4 volts/cm. In-plane conductivities (σ_s) using microcircuit arrays can be estimated in this linear regime according to

$$\sigma_s = \frac{j}{V} L \quad , \tag{1}$$

where j is the current density, V the applied potential, and L the electrode spacing in centimeters (10^{-3} cm for these circuits).[13,14,38–40] Dark conductivities for 28 bilayer films of Pc **1** were approximately 10^{-10} $\Omega^{-1}cm^{-1}$ for $\sigma_\perp$ and ranged from 2×10^{-10} to 5×10^{-9} $\Omega^{-1}cm^{-1}$ for σ_{II}, with anisotropies in dark conductivity in this ohmic regime: $2 \leqslant \sigma_{II}/\sigma_\perp \leqslant 50$ (Table I). Twenty-eight bilayer films of Pc **1'** displayed similar j-V behavior with $10 \leqslant \sigma_{II}/\sigma_\perp \leqslant 20$ in the ohmic regime. Similar anisotropies in current have been measured on ordered films of hexabenzocoronene derivatives by Warman and co-workers using time resolved microwave conductivity.[41]

At potentials above 15 volts the current–voltage behavior for all Pc films exhibited space-charge-limited current (SCLC) behavior at fields exceeding 10^4 volts/cm.[38–40,42] We assume a dielectric constant for the material, $\varepsilon \approx 2$,[43] and use the slope of the linear j_{SCLC} versus V^2 plots (Fig. 3) to estimate mobilities (μ) for these thin film materials according to Child's Law

$$j_{SCLC} = \frac{9}{8} \epsilon_0 \epsilon \mu \frac{V^2}{d^3} \quad , \tag{2}$$

where j_{SCLC} is the current density in the SCLC regime, ε_o is the permittivity of free space, V is the potential, and d is the separation between the electrodes (10^{-3} cm).[43] Charge carrier mobilities exceeded 10^{-4} $cm^2 \cdot V^{-1} \cdot s^{-1}$ (holes are the majority charge carrier in these easily oxidized systems) and electrical anisotropies as high as 50:1 ($\sigma_{II}/\sigma_\perp$) were observed.[37]

The variability in these responses was significant, especially for conductivity measurements along the column axis direction, with current densities varying by as much as a factor of 10× from microcircuit to microcircuit. We attribute this variability to the difficulty in making uniform electrical contacts to the entire Pc film, owing to the variability in "cutting" these thin films with the microcircuits during horizontal film transfer. The increases in conductivity, mobilities, and electrical anisotropy reported here versus those reported previously for other rod-like Pc assemblies[12–14] likely arise from enhanced long-range order in the Pc columns, owing to the nature of the interactions between side chains and the surface modification protocols adopted to prepare the microcircuit substrate for proper wetting and transfer of the Pc aggregates.

The photoconductivities of these materials were also explored. Figures 2(c) and 2(d) show several current/voltage plots for films of both **1** and **1'** using either He–Ne laser (15 mW) or a filtered white light source (430 mW) in the ohmic regime. Photocurrent densities with HeNe excitation varied from 0.02 to 0.5 mA cm^{-2} for films of Pc **1** and **1'**, respectively, the ratio of photo-to-dark conductivities was as high as 50, and anisotropies

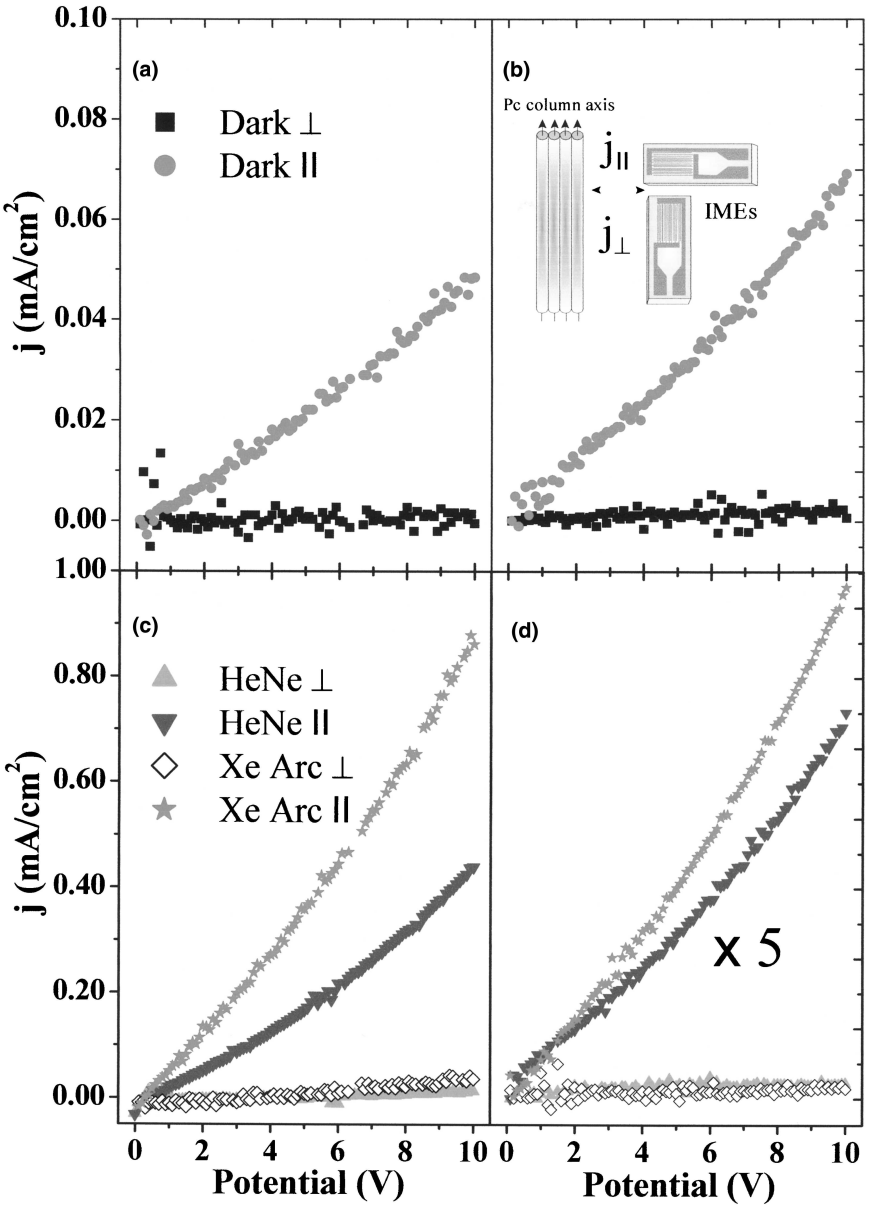

FIG. 2. Current density versus voltage curves recorded for (a) 28 bilayer films of **1** and (b) 28 bilayer films of **1'** on pairs of microelectrode array circuits. Dark current responses to applied potentials in orthogonal orientations are shown as $j_{\perp}$ (■) and $j_{\parallel}$ (●). Photocurrent densities versus voltage curves for (c) 28 bilayer films of **1** and (d) 28 bilayer films of **1'** under HeNe laser illumination are shown as $j_{\perp}$ (▲) and $j_{\parallel}$ (▼) and photocurrent densitites under Xe arc lamp irradiation as $j_{\perp}$ (◇) and $j_{\parallel}$ (★).

in photoconductivity ranged from $10 \leqslant \sigma_{II}/\sigma_{\perp} \leqslant 70$. During excitation with the filtered white light source, current densities were as much as a factor of 20× higher, and $\sigma_{II}/\sigma_{\perp}$ ranged from 6 to 98.

B. dc conductivities of Pc 2

As discussed in recent reports,[17] the annealed but unpolymerized films of Pc **2** show dark conductivities, hole mobilities, and values of $\sigma_{II}/\sigma_{\perp}$ comparable to annealed films of Pc **1**. After irradiation of films of **2** for 5 h, however, dark conductivities increased parallel to the column axis and decreased perpendicular to the column axis, causing $\sigma_{II}/\sigma_{\perp}$ ratios to increase by 10× relative to prephotolysis values. From the slopes of j versus V^2 plots in the SCLC regime, we estimate hole mobilities as high as 1.7×10^{-3} $cm^2 \cdot V^{-1} \cdot s^{-1}$ for photolyzed films of **2**.[37,38] The most likely explanation for this increase in apparent mobility is the removal of trap sites due to structural defects in the bulk of the Pc film, which is where most of the current flows in these IME circuits. Whether there is some interdigitation of the side chains on adjacent columns upon polymerization is not clear and is the subject of current studies using conductive tip AFM on a submicrometer distance scale.

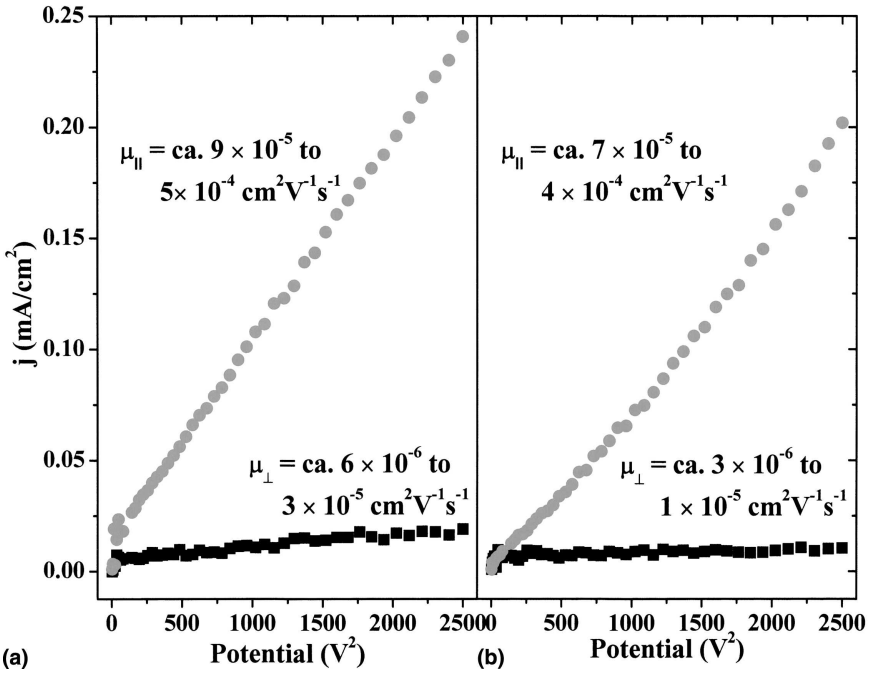

FIG. 3. Current density versus the square of the applied voltage for bilayer films of (a) Pc **1** and (b) Pc **1'** on orthogonal pairs of IME array circuits in the space-charge limited currents regime. Mobilites ($\mu_\perp$ and $\mu_{||}$) were estimated from the slopes of these plots [Child's Law, Eq. (2)].

C. OFET behavior for films of Pc 1 and Pc 2

OFET devices with both thin films of **1** and **2** as the organic semiconductor showed typical transistor behavior with a linear i/V region at low V_D and a saturation region at higher drain voltages (V_D) [Figs. 4(a) and 5(b)]. Mobilities were calculated in the linear region of the curve, which is described by the following equation at low V_D

$$I_D = \frac{WC_i\mu}{L}\left(V_G - V_T - \frac{V_D}{2}\right)V_D \quad , \qquad (3)$$

where I_D is the drain current, W and L are the width (distance end to end) and length (separation) of the source and drain electrodes, C_i is the capacitance per unit area, μ is the field-effect mobility, V_G is the gate voltage, and V_T is the threshold voltage. Charge mobilities are extracted from this region of the curve by calculating the transconductance (g_m)

$$g_m = \left.\frac{\delta I_D}{\delta V_G}\right|_{V_D=\text{const.}} = \frac{WC_i}{L}\,\mu V_D \quad . \qquad (4)$$

Contact resistances were extracted from a plot of the total device resistance (calculated from Ohm's law in the linear region of the I_D versus V_D plot) versus the device length extrapolated to a length of zero.[44] This extracts the contact resistance from the total device resistance, which also includes resistances from the semiconductor itself and grain boundaries within the semiconductor. Both the mobilities and the contact resistances for the OFETs based on Pc **1** exhibited a wide range of values, as with the microcircuit dc conductivity experiments, which we attribute to irregular contact between the Pc film and the source-drain electrodes in each device. Typical mobilities (measured over approximately 20 devices) were between 1×10^{-6} $cm^2 \cdot V^{-1} \cdot s^{-1}$ and 5×10^{-6} $cm^2 \cdot V^{-1} \cdot s^{-1}$, and contact resistances were between 10^9 and 10^{10} Ω. These contact resistance values are similar to those measured by Frisbie and co-workers in small molecule transistors (sexithiophene and pentacene),[27–28] but are considerably higher than those measured on a poly(3-hexylthiophene) by Bürgi and coworkers.[45]

Figure 5(a) focuses on an analysis of the source-drain currents for OFETs created from Pc **1**, at $V_D = V_G = -20$ volts (near saturation conditions). Devices are compared where the columnar aggregates were deposited so that current would flow either parallel or perpendicular to the Pc columns [as in Fig. 2(b)]. In this generation of OFET devices the saturation current parallel to the Pc column axis ($I_{D,||}$) is approximately 10× higher than that perpendicular to the columns ($I_{D,\perp}$). The uncertainty in measuring $I_{D,\perp}$ is higher (noise in the measured current was greater) than for $I_{D,||}$. As will be discussed below, the fact that the ratio $I_{D,||}/ I_{D,\perp}$ is constant with W/L ratio suggests that the fraction of Pc columns that make good contact to the source-drain electrodes, and therefore contribute to the OFET activity of these thin films, is *approximately* constant with electrode dimension (but with considerable variability), down to the smallest electrodes explored in this study.

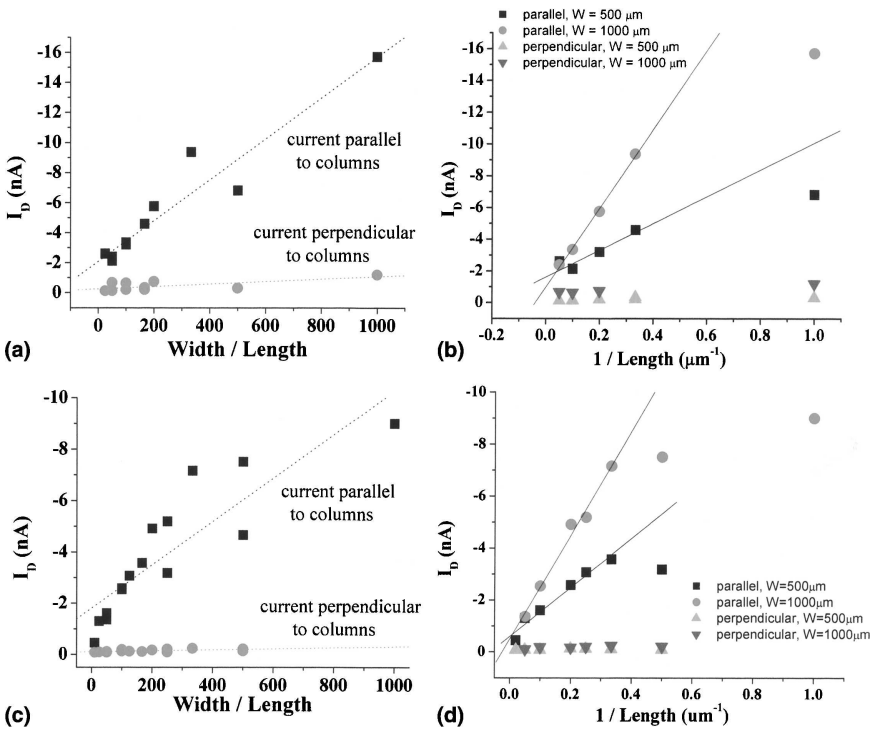

FIG. 4. I_D (at saturation conditions) versus W/L plot for annealing films of (a) **1** and (c) **2** for two OFET chips prepared together so that currents travel either parallel or perpendicular to the column axis. The anisotropy in drain currents was about 10× higher along the column axis than across it for films of **1** and about 10–30 times higher for films of **2.** I_D versus 1/L plots (b) and (d) for Pcs **1** and **2,** show that at low channel lengths, currents are lower than predicted by Eq. (5). The lines are linear fits to the data excluding the data point for L = 1 μm.

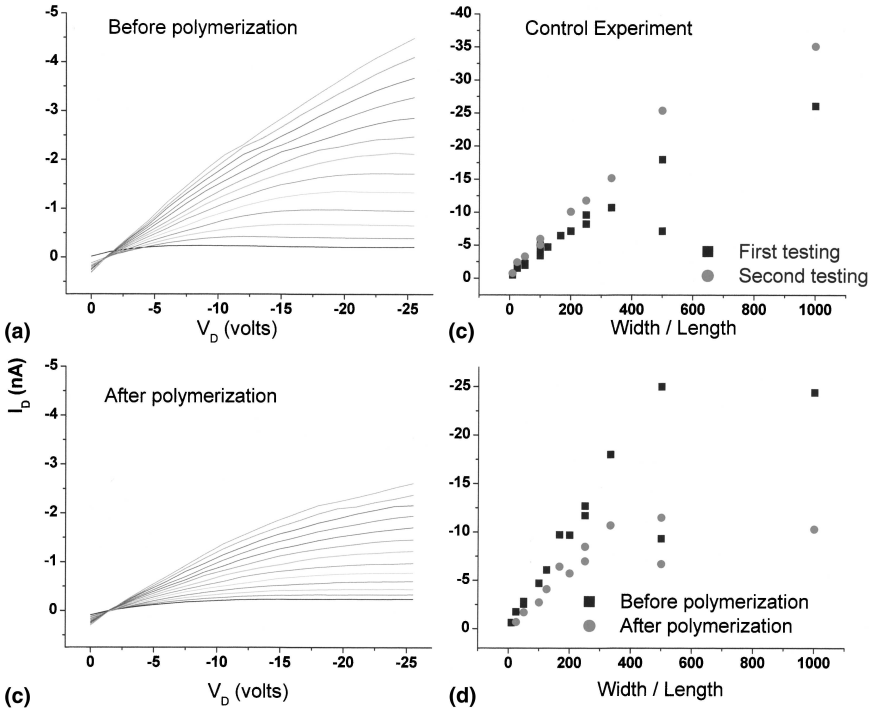

FIG. 5. I_D versus V_D curved from V_G = 0v to –25 V for the same 7 monolayer film of **2** (a) before polymerization and (b) after polymerization on a device with W = 1000 μm and L = 10 μm. There is a clear decrease in the current following polymerization. (c) and (d) show I_D versus W/L plots summarizing the data for all of the transistors measured. (c) Shows the data for a control set of transistors that were tested about 24-h apart without treatment. (d) Shows the data for the experimental set of transistors that were polymerized between testings. Currents in (c) and (d) were measured at a V_D = –25.5 V and V_G = 25V.

Anisotropy measurements were also made on annealed films of **2** with currents measured both parallel and perpendicular to the column axis. Similar to films of **1**, the currents measured perpendicular to the column axis were very noisy. Drain currents measured at $V_D = V_G = -20$ V are plotted as a function of W/L for the devices with films of **2** in Fig. 5(c). These currents also fell along two lines depending on the direction of current flow; currents were on average 10–30 times higher along the column axis than across it. The range of anisotropies for films of **2** is higher than that observed for films of **1**, suggesting that these as-deposited films exhibit more well ordered columnar structures on these substrates.

The effect of reducing the channel length in these OFETs is shown in plots of I_D versus 1/L in Figs. 5(b) and 5(d). It is clear that the current in the longer channels follows a linear trend as described by Eq. (5)

$$I_D = \frac{WC_i\mu}{2L}(V_G - V_t)^2 \quad . \tag{5}$$

In the 1-μm channel, however, the currents are lower than predicted. This effective current decrease for short channels has been observed previously and has been attributed to the relatively larger fraction of V_D that is lost due to a voltage drop at the contacts due to contact resistance.[46]

The effect of polymerization on these films was probed by preparing and testing two identical samples, polymerizing one of the samples, and then retesting both samples. In this way, the sample that was not polymerized acted as a control to determine the effect of testing and handling on the electrical properties of the film. Figures 4(a) and 4(b) shows I_D versus V_D curves for a device on the chip that was polymerized, before and after this polymerization process. After polymerization, the currents actually decreased by approximately 50%, in contrast to dc conductivity experiments previously reported.[17] Figures 4(c) and 4(d) summarize this data for a range of devices in a plot of I_D (at $V_D = -25.5$ V and $V_G = -25$ V) versus W/L for both the control film [Fig. 4(c)] and the polymerized film [Fig. 4(d)]. The control experiment showed a slight but consistent increase in current for the second testing, most likely due to oxygen doping in the films, which is well documented in phthalocyanine materials, due to the slow introduction with time of partially oxidized Pcs, which act to "dope" the Pc film.[47–50] This doping acts to increase the drain currents but decrease the degree of saturation with time. Currents on the second chip, which underwent irradiation with 254-nm light to polymerize the film, consistently showed a decrease in current following the polymerization process [Fig. 4(d)], which as the control experiment demonstrated was not due to film testing and handling. We have previously verified that films of **2** do not suffer decomposition during these polymerization steps, as they are carried out in Ar saturated environments, and there is no loss of Q-band absorbance intensity in these films over time.[17,37,38] From experiments done to date we conclude that for Pc films of this thickness, on these OFET substrates, microstructural changes during the polymerization event actually cause a partial loss of contact to the source/drain electrodes in the region of the Pc film near the oxide substrate.[17] Experiments with top contacts to these materials, extensively modified substrates, and measurements on sub-micron length scales, are underway to further explore this phenomenon.

It has been shown in OFET studies of other organic materials that there may be some benefit in modification of the Au source/drain contacts with substituted thiols, to improve both wettability and decrease charge injection barriers.[51–53] We are evaluating similar strategies with these columnar Pc films, but have had our best results with 4-mercaptopyridine [see inset of Fig. 6(c)], which is expected to orient a pyridine moiety (a weak ligand for d_{10} metals such as copper in the Pc core) so that the nitrogen is exposed to the termini of the Pc columnar aggregates at the boundaries of the Pc film. Figures 6(a) and 6(b) show I_D versus V_D curves for a transistor with bare electrodes and modified electrodes, respectively. In general, the current at any bias increased by a factor of approximately 4× for devices modified with 4-mercaptopyridine. This data is summarized for more of the transistors tested in Fig. 6(c) where the drain current (at $V_D = -25.5$ V and $V_G = -26$ V) is plotted versus W/L to illustrate that this trend continues for all of the devices measured. Contact resistances for these devices, however, continued to show considerable variability, and additional Au modifiers and modified Pcs are being evaluated to further improve these i/V characteristics.

Silane modifications of gate oxides in OFETs, prior to deposition of organic semiconductors, has also been shown to provide for better transistor behavior.[53–55] Indeed, our own previous experiments have shown that modification of oxide/Si(100) surfaces with specific silanes (especially those with phenyl termination) produces a more coherent film of Pc **1** and **2**,[17–20,37,38] and those modification procedures were evaluated in our first generation OFET experiments. In the experiments conducted to date, however, no dramatic increase in I_D or charge mobilities were observed as a result of those modifications to the gate oxide. More experiments are clearly warranted to further evaluate these modification steps where the OFET behavior is evaluated on smaller length scales and with top contacts.

D. Conductive tip AFM characterization of electrical properties of thin films of Pc 1

The challenges to obtaining high charge mobilities from these discotic mesophase materials in OFET

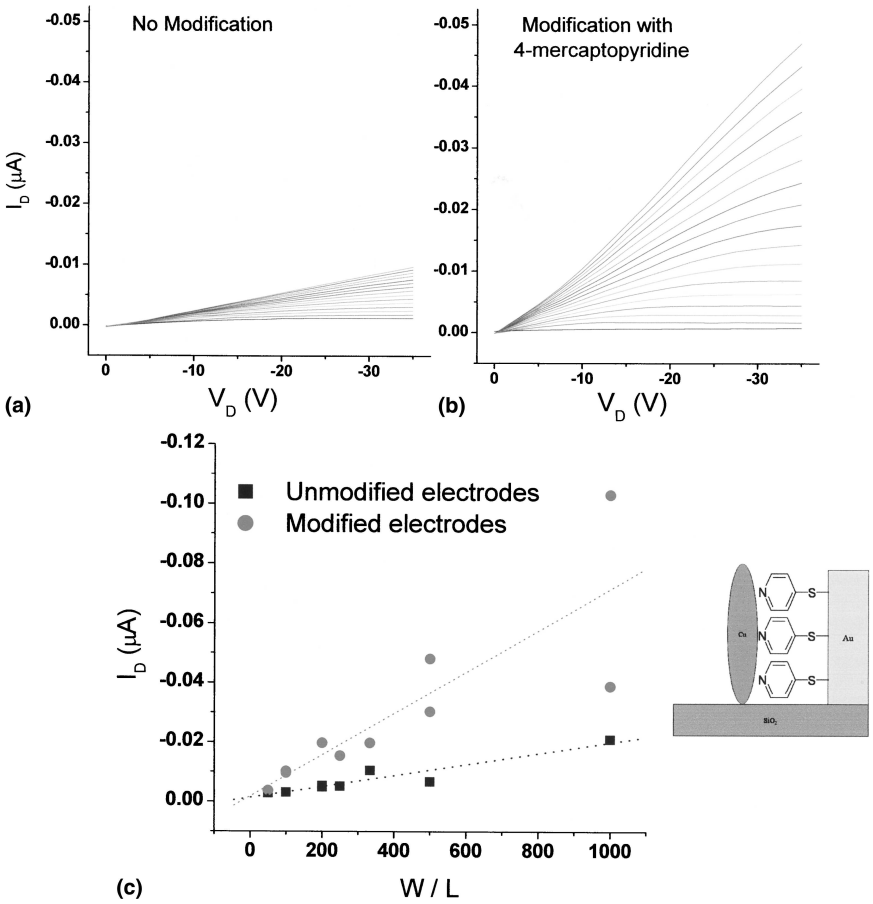

FIG. 6. I_D versus V_D curves from V_G = +5 V to –35 V for a 7 monolayer film of 2 (a) with unmodified source and drain electrodes and (b) with source and drain electrodes modified with 4-mercaptopyridine on a device with W = 1000 μm and L = 5 μm. There is a clear increase in the current on the device with modified electrodes. (c) This data is further summarized in a plot of I_D versus W/L (at V_D = −25.5 V and V_G = −26V) for the devices with W = 1000 μm and shows that this trend holds for all of the devices tested.

technologies are revealed in conductive tip AFM characterization on the submicrometer distance scale. Figure 7 shows the current–voltage curves for a 4-bilayer film of Pc **1** deposited on a 100 nm SiO_2/Si(100) wafer, where a 2 mm × 2 mm Au bond pad acted as one electrode and a Pt/Ir AFM tip acted as the opposite electrode. Several current–voltage curves were recorded, as the distance between the tip and the bond pad was varied from approximately 10 μm to approximately 0.1 μm, approaching from both directions parallel to the Pc column axis and perpendicular to the Pc column axis [schematic views in Fig. 7(b)]. At tip-to-pad distances in excess of approximately 1 μm, parallel to the Pc column axis [schematically shown as point 1 in Fig. 7(b)], or at any tip-to-pad distance perpendicular to the column axis (e.g., points 3 and 4 in Fig. 7), the current-voltage response was linear (ohmic regime), and the measured currents were not bigger than 0.2 pA at an applied voltage of 10 volts. In selected regions of the Pc film, measurements along the column axis at tip-to-pad distances less than 0.5 μm (e.g., point 2) produced significantly different current–voltage behavior, with adistinct nonlinear increase in current density above applied fields of approximately 10^5 volts/cm. There was some rectification in the i/V response, suggesting that the barriers to charge injection at the Pt/Ir and Au contacts are not equal.[39,40] Comparing the currents at points on the Pc film (such as point 2 versus point 4) anisotropies in conductivity ranged from 50:1 up to 1000:1. Current versus V^2 plots were obtained at point 2 and similar points near the Au bond pad, parallel to the Pc column axis from which estimates of charge mobilities were made. The calculated mobilities have considerable uncertainty due to the unknown contact area of the tip, and the degree of contact between the Pc film and the Au bond pad. The tip area has been estimated from the known geometries of the AFM tips used,[38] and assumptions as to the penetration depth of the tip into the sample during the actual measurement. Assumed tip contact areas for penetration through one monolayer, or through all 4 bilayers, give electrode surface areas of 14 nm^2 and 200 nm^2, respectively. Using these areas in Eq. (2) provides a range of

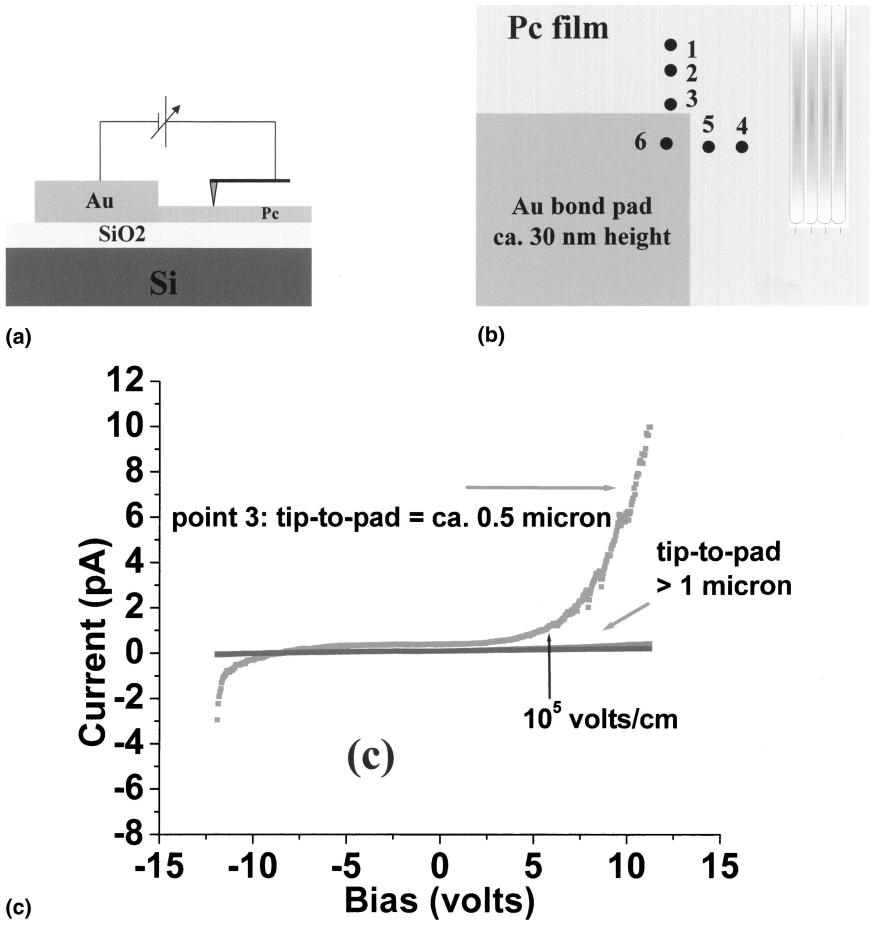

FIG. 7. Dark conductives of a two bilayer film of Pc **1** on silicone oxide using a gold bond pad for one the the electrodes and a Pt/Ir AFM tip as the other electrode. This schematic side view of this experiment is shown in (a), and a schematic of the positions of the tip with respect to the bond pad are shown in (b). Data was taken at several points approaching the bond pad, so that the conductivity axis was parallel to the Pc column axis (points 1 and 2) or perpendicular to the Pc column axis (points 3 and 4). i/V curves are shown in (c) for current flowing parallel to the column axis at distances of ca. 0.5 μm (point 1) and at distances greater than 1 μm (point 2).

mobilities from these measurements of 0.01 to 0.2 $cm^2 \cdot V^{-1} \cdot s^{-1}$, which is higher than those measured using the IMEs, and significantly higher than the field effect mobilities measured with the OFETs.

Comparisons between the conductive tip AFM and OFET measurements are difficult to make. Figures 5(b) and 5(d) illustrated an effective current decrease at the L = 1-μm devices, however, the mobilities measured on the L = 500-nm scale in the AFM studies are clearly much higher. The significantly different geometries (W/L ratio) of these experiments may be the cause for these differences, as W/L can be as low as 0.01 for the AFM experiment and can be as high as 1000 for the OFET experiments. High mobilities in the conductive tip AFM experiment, however, are not unexpected given the small length scale of the measurement (close to the average length of the most coherent Pc columns we have seen by AFM measurement), and the small area of the film that is being investigated (only a few adjacent columns).

The high currents and charge mobilities were only seen on a fraction of the Pc film deposited by horizontal transfer to these substrates. As might be expected, ohmic contact between the rod ends in these Pc films and the walls of the Au pads is not achieved over large areas, suggesting that the i/V responses in Figs. 2–6 above are achieved from only approximately 5–10% of the total Pc film area. Images of the current, at a bias of 7 volts, were taken over large areas of the Pc film near the Au contacts, and bright regions (currents like that shown for point 2 in Fig. 7) were seen at distances within 0.5 μm of the bond pad, only for directions parallel to the Pc columns, and only for approximately 5–10% of the Pc film regions close to these bond pads.[38] Further experiments of this type are underway with modification of both the gate oxide and the source/drain electrodes to determine the

conditions under which enhanced contact, and enhanced coherence of the Pc films can be achieved.

IV. CONCLUSIONS

The formation of well-organized discotic mesophase materials into rod-like columnar aggregates has intrinsic appeal for OFET systems, provided that these materials can be organized sufficiently over reasonable coherence lengths to take advantage of the high mobilities along the column axis and that ohmic contacts can be readily made to the column ends. To date, including the work presented here, these systems have not shown the performance characteristics of other vacuum-deposited or solution deposited small molecule systems, especially when compared with recent reports of pentacene and oligothiophene transistors with exceptionally high mobilities.[56–58]

It is clear that we can obtain columnar aggregates with coherence lengths up to approximately 150 nm, and anisotropies in electrical conductivity and current ($\sigma_{II}/\sigma_{\perp}$ and $I_{D,\|}/ I_{D,\perp}$) which are 10–100, when measured on the 2–10-μm length scale, and up to 1000 for dc conductivities measured on the submicrometer length scale. The role of the side chains in preventing flow of charges perpendicular to the columns appears to be constant when characterized on the micrometer length scale, as revealed in our OFET studies with variable length and widths in these circuits. The implication is that a constant fraction of the Pc columns are oriented to maximize charge mobilities along the column axis [inset (a) in Fig. 1], and similarly, a constant fraction within each film is disordered to such an extent to allow current to flow perpendicular to that direction [inset (b) in Fig. 1].

If film properties can be further optimized to achieve greater coherence, with a higher fraction of the Pc columns oriented along the desired current axis, and if the source/drain electrode gap (L) can be routinely reduced to submicrometer length scales, we can anticipate much higher field effect mobilities for LB-deposited thin films. Experiments to verify this hypothesis are underway, as is the characterization of new Pc materials with modified side chains that make them amenable to thin film spin-casting or solution casting, where ordering is achieved after film deposition.

ACKNOWLEDGMENTS

Research support is gratefully acknowledged from the National Science Foundation Center for Materials and Devices for Information Technology, DMR-0120967 (N.R.A., B.K., and D.L.M.), NSF-Chemistry-0211900 (N.R.A.), Pfizer Corporation (Graduate Fellowship to C.L.D.), and Procter and Gamble (ACS Division of Analytical Chemistry Graduate Fellowship to C.L.D.). The authors also gratefully acknowledge Dr. Peter Harris, Veeco-Digital Instruments, for his assistance in obtaining the initial C-AFM data.

REFERENCES

1. A.M. van de Craats and J.M. Warman: *Adv. Mater.* **13,** 130 (2001).
2. A.M. van de Craats, J.M. Warman, J.M.A. Fechtenkotter, J.D. Brand, M.A. Harbison, and K. Mullen: *Adv. Mater.* **11,** 1469 (1999).
3. A.M. van de Craats, J.M. Warman, K. Mullen, Y. Geerts, and J.D. Brand: *Adv. Mater.* **10,** 36 (1998).
4. A.M. van de Craats, L.D.A. Siebbeles, I. Bleyl, D. Haarer, Y.A. Berlin, A.A. Zharikov, and J.M. Warman: *J. Phys. Chem. B* **102,** 9625 (1998).
5. A.M. van de Craats, J.M. Warman, H. Hasebe, R. Naito, and K. Ohta: *J. Phys. Chem. B* **101,** 9224 (1997).
6. L. Schmidt-Mende, M. Watson, K. Mullen, and R.H. Friend: *Molecular Crystals and Liquid Crystals* **396,** 73 (2003).
7. K. Petritsch, J.J. Dittmer, E.A. Marseglia, R.H. Friend, A. Lux, G.G. Rozenberg, S.C. Moratti, and A.B. Holmes: *Sol. Energy Mater. Sol. Cells* **61,** 63 (2000).
8. P. Samori, N. Severin, K. Mullen, and J.P. Rabe: *Adv. Mater.* **12,** 579 (2000).
9. H. Eichhorn: *J. Porphyrins Phthalocyanines* **4,** 88 (2000).
10. A. Tracz, J.K. Jeszka, M.D. Watson, W. Pisula, K. Mullen, and T. Pakula: *J. Am. Chem. Soc.* **125,** 1682 (2003).
11. O. Bunk, M.M. Nielsen, T.I. Solling, A.M. van de Craats, and N. Stutzmann: *J. Am. Chem. Soc.* **125,** 2252 (2003).
12. S.J. Tans, R.G. Miedema, L.J. Geerligs, C. Dekker, J. Wu, D. Neher, and G. Wegner: *Nanotechnology* **14,** 1043 (2003).
13. P. Gattinger, H. Rengel, D. Neher, M. Gurka, M. Buck, A.M. van de Craats, and J.M. Warman: *J. Phys. Chem. B* **103,** 3179 (1999).
14. R. Silerova, L. Kalvoda, D. Neher, A. Ferencz, J. Wu, and G. Wegner: *Chem. Mater.* **10,** 2284 ((1998)).
15. M.A. Fox, J.V. Grant, D. Melamed, D.T. Torimoto, C.Y. Liu, and A.J. Bard: *Chem. Mater.* **10,** 1771 (1998).
16. C-Y. Liu and A.J. Bard: *Acc. Chem. Res.* **32,** 235 (1999).
17. C.L. Donley, W. Xia, B.A. Minch, R.A.P. Zangmeister, A.S. Drager, K. Nebesny, D.F. O'Brien, and N.R. Armstrong: *Langmuir* **19,** 6512 (2003).
18. R.A.P. Zangmeister, D.F. O'Brien, and N.R. Armstrong: *Adv. Func. Mater.* **12,** 179 (2002).
19. R.A.P. Zangmeister, P.E. Smolenyak, A.S. Drager, D.R. O'Brien, and N.R. Armstrong: *Langmuir* **17,** 7071 (2001).
20. P. Smolenyak, R. Peterson, K. Nebesny, M. Torker, D.F. O'Brien, and N.R. Armstrong: *J. Am. Chem. Soc.* **121,** 8628 (1999).
21. L. Torsi, A. Dodabalapur, L.J. Rothberg, A.W.P. Fung, and H.E. Katz: *Science* **272,** 1462 (1996).
22. Z. Bao, A.J. Lovinger, and A. Dodabalapur: *Appl. Phys. Lett.* **69,** 3066 (1996).
23. H.E. Katz and Z. Bao: *J. Phys. Chem. B* **104,** 671 (2000).
24. J.A. Rogers, A. Dodabalapur, Z. Bao, and H.E. Katz: *Appl. Phys. Lett.* **75,** 1941 (1999).
25. A.B. Chwang and C.D. Frisbie: *J. Appl. Phys.* **90,** 1342 (2001).
26. T.W. Kelley and C.D. Frisbie: *J. Phys. Chem. B* **105,** 4538 (2001).
27. K. Seshadri and C.D. Frisbie: *Appl. Phys. Lett.* **78,** 993 (2001).
28. A.B. Chwang and C.D. Frisbie: *J. Phys. Chem. B* **104,** 12202 (2000).

29. E.L. Granstrom and C.D. Frisbie: *J. Phys. Chem. B* **103,** 8842 (1999).
30. C.D. Dimitrakopoulos and P.R.L. Malenfant: *Adv. Mater.* **14,** 99 (2002).
31. G. Horowitz: *Adv. Mater.* **10,** 365 (1998).
32. G. Horowitz, R. Hajlaoui, H. Bouchriha, R. Bourguiga, and M. Hajlaoui: *Adv. Mater.* **10,** 923 (1998).
33. H. Klauk and T.N. Jackson: *Solid State Technol.* **43,** 63 (2000).
34. H. Klauk, G. Schmid, W. Radlik, W. Weber, L.S. Zhou, C.D. Sheraw, J.A. Nichols, and T.N. Jackson: *Solid-State Electron.* **47,** 297 (2003).
35. Y. Zhang, J.R. Petta, S. Ambily, Y. Shen, D.C. Ralph, and G.G. Malliaras: *Adv. Mater.* **15,** 1632 (2003).
36. A.S. Drager and D.F. O'Brien: *J. Org. Chem.* **65,** 2257 (2000).
37. R.A.P. Zangmeister: Ph.D. Thesis, University of Arizona (2001).
38. C.L. Donley: Ph.D. Thesis, University of Arizona (2003).
39. F. Gutman: *Organic Semiconductors* (John Wiley & Sons, New York, 1967).
40. J.D. Wright, *Molecular Crystals* (Cambridge University Press, New York, 1995), pp. 144–158.
41. J. Piris, M.G. Debije, N. Stutzmann, A.M. van de Craats, M.D. Watson, K. Müllen, and J.M. Warman: *Adv. Mater.* **15,** 1736 (2003).
42. J. Simon and J.-J. André, *Molecular Semiconductors* (Springer-Verlag, New York, 1985), pp. 53–59).
43. *CRC Handbook of Chemistry and Physics*, 71st ed. (CRC Press, Boca Raton, 1990).
44. P.V. Necliudov, M.S. Shur, D.J. Gundlach, and T.N. Jackson: *Solid-State Electron.* **47,** 259 (2003).
45. L. Bürgi, H. Sirringhaus, and R.H. Friend: *Appl. Phys. Lett.* **80,** 2913 (2002).
46. E.J. Meijer, G.H. Gelinck, E. van Veenendaal, B-H. Huisman, D.M. de Leeuw, and T.M. Klapwijk: *Appl. Phys. Lett.* **82,** 4576 (2003).
47. J.W. Pankow, C. Arbour, J-P. Dodelet, G.E. Collins, and N.R. Armstrong: *J. Phys. Chem.* **97,** 8485 (1993).
48. I. Zhivkov, S. Nešpůrek, and F. Schauer: *Adv. Mater. Opt. Electron* **9,** 175 (1999).
49. A. Ahmad and R.A. Collins: *Thin Solid Films* **217,** 75 (1992).
50. A. Ferencz, N.R. Armstrong, and G. Wegner: *Macromolecules* **27,** 1517 (1994).
51. H.E. Katz, J. Johnson, A.J. Lovinger, and W.J. Li: *J. Am. Chem. Soc.* **122,** 7787 (2000).
52. H. Klauk, M. Halik, U. Zschieschang, G. Schmid, W. Radlik, and W. Weber: *J. Appl. Phys.* **92,** 5259 (2002).
53. T.W. Kelley, L.D. Boardman, R.D. Dunbar, D.V. Muyres, M.J. Pellerite, and T.P. Smith: *J. Phys. Chem. B* **107,** 5877 (2003).
54. Y.Y. Lin, D.J. Gundlach, S.F. Nelson, and T.N. Jackson: *IEEE Elect. Dev. Lett.* **18,** 606 (1997).
55. A. Salleo, M.L. Chabinyc, M.S. Yang, and R.A. Street: *Appl. Phys. Lett.* **81,** 4383 (2002).
56. G.Z. Wang, Y. Luo, and P.H. Beton: *Appl. Phys. Lett.* **83,** 3108 (2003).
57. M. Mushrush, A. Facchetti, M. Lefenfeld, H.E. Katz, and T.J. Marks: *J. Am. Chem. Soc.* **125,** 9414 (2003).
58. H. Meng, J. Zheng, A.J. Lovinger, B.C. Wang, P.G. Van Patten, and Z.N. Bao: *Chem. Mater.* **15,** 1778 (2003).